An amplified electrochemical sensor employing one-step synthesized nickel–copper–zinc ferrite/carboxymethyl cellulose/graphene oxide nanosheets composite for sensitive analysis of omeprazole†

Biuck Habibi, [iD] *[a] Sara Pashazadeh, [iD] [a] Ali Pashazadeh [iD] [a] and Lotf Ali Saghatforoush [iD] [b]

In this work, a signal amplification strategy was designed by the fabrication of a highly sensitive and selective electrochemical sensor based on nickel–copper–zinc ferrite ($Ni_{0.4}Cu_{0.2}Zn_{0.4}Fe_2O_4$)/carboxymethyl cellulose (CMC)/graphene oxide nanosheets (GONs) composite modified glassy carbon electrode (GCE) for determination of omeprazole (OMP). The one-step synthesized $Ni_{0.4}Cu_{0.2}Zn_{0.4}Fe_2O_4$/CMC/GONs nanocomposite was characterized by scanning electron microscopy, energy-dispersive X-ray spectroscopy, transmission electron microscopy and X-ray diffraction techniques. Then, the $Ni_{0.4}Cu_{0.2}Zn_{0.4}Fe_2O_4$/CMC/GONs/GCE was applied to study the electrochemical behavior of the OMP. Electrochemical data show that the $Ni_{0.4}Cu_{0.2}Zn_{0.4}Fe_2O_4$/CMC/GONs/GCE exhibits superior electrocatalytic performance on the oxidation of OMP compared with bare GCE, GONs/GCE, CMC/GONs/GCE and MFe_2O_4/GCE (M = Cu, Ni and Zn including single, double and triple of metals) which can be attributed to the synergistic effects of the nanocomposite components, outstanding electrical properties of $Ni_{0.4}Cu_{0.2}Zn_{0.4}Fe_2O_4$ and high conductivity of CMC/GONs as well as the further electron transport action of the nanocomposite. Under optimal conditions, the $Ni_{0.4}Cu_{0.2}Zn_{0.4}Fe_2O_4$/CMC/GONs/GCE offers a high performance toward the electrodetermination of OMP with the wide linear-range responses (0.24–5 and 5–75 μM), lower detection limit (0.22 ± 0.05 μM), high sensitivity (1.1543 μA μM^{-1} cm^{-2}), long-term signal stability and reproducibility (RSD = 2.54%). It should be noted that the $Ni_{0.4}Cu_{0.2}Zn_{0.4}Fe_2O_4$/CMC/GONs/GCE sensor could also be used for determination of OMP in drug and biological samples, indicating its feasibility for real analysis.

1. Introduction

Omeprazole (OMP), {5-methoxy-2-[(4-methoxy-3,5-dimethylpyridin-2-yl) methanesulfinyl]-1*H*-benzimidazole}, a substituted benzimidazole compound, is one of the first proton pump inhibitors to reduce gastric acid secretion and the prevention and treatment of gastric, duodenal ulcers or gastric reflux, as well as the treatment of infections caused by *Helicobacter pylori* (*H. pylori*).[1–3] Also, a triple treatment regimen with OMP, amoxicillin, and clarithromycin has also been widely used to eradicate *H. pylori*.[4–6] In fact, OMP is a pro-drug that is converted to an active sulfenamide intermediate at low pHs that binds to the thiol groups of the gastric wall proton pump cell (H^+/K^+-ATPase).[3,7,8] Due to the importance of measuring OMP as well as the widespread commercialization of OMP-containing drug formulations, a wide range of analytical techniques including spectrophotometric,[7,9–11] electrophoretic,[8,12] chromatographic[13–17] and electroanalytical methods[18–23] have been reported to its evaluation. Spectroscopic and chromatographic methods to measure the OMP often require complicated and tedious sample preparation, pretreatment processes, expensive materials, and advanced instruments.[24] While, the electroanalytical methods (electrochemical sensors) are simple, fast, cheap, accurate and minimal sample preparation, as well as powerful and practical techniques for analyzing with high selectivity, sensitivity, reproducibility, quick response time, and cheap instrumentation.[25] Electrochemical sensors performances are limited due to slow electron transfer kinetics and the high required overpotential for the redox reaction of analyte molecules or ions. To illuminate these problems, the electrode surface should be modified with suitable materials to increase

[a]*Electroanalytical Chemistry Laboratory, Department of Chemistry, Faculty of Sciences, Azarbaijan Shahid Madani University, Tabriz 53714-161, Iran. E-mail: biuckhabibi.a@gmail.com; Fax: +98 41 34327541; Tel: +98 41 31452135*

[b]*Department of Chemistry, Payame Noor University, 19395-4697 Tehran, I. R. Iran*

its electroactivity, sensitivity, and selectivity.[26] Nowadays, nanomaterials as electrode materials are the most suitable materials for electrode modifiers, which have great potential for developing new devices and designing sensors with unique capabilities.[27] Nanomaterial-based electrochemical sensors have great potential for enhancing electrical, physical, and sensing performance, especially in terms of selectivity and sensitivity.[28] Hence, significantly and extensive researches on the fabrication of functional electrode materials, along with numerous electrochemical methods, are driving the widespread application of electrochemical devices. Compared to other nanoparticles, magnetic nanoparticles with the general formula MFe_2O_4-type spinel nano ferrites (M = is a divalent cation such as Fe, Co, Cu, Ni, *etc.*), a group of inorganic biomaterials, that are the most well-known compounds in analytical biochemistry, medicine, biotechnology and separation methods.[29] Due to their good biocompatibility, good electrocatalytic properties, low toxicity, and easy preparation, these nanoparticles have received more attention in the preparation of sensors and biosensors.[30–32] Ferrites are the most promising compounds among magnetic oxide complexes, which have complexes of iron oxides with different crystalline structures. There are currently several types of ferrites including spinel's ferrites, hexagonal ferrites, garnets, and ortho ferrites. Among these ferrites, spinel ferrites with hydrophilic nature are important magnetic materials due to their outstanding magnetic and electrical properties.[33–35] One of the most essential spinel ferrites that has a mixed spinel structure is the Ni–Cu–Zn nano-crystalline ferrite. The nano-crystalline Ni–Cu–Zn ferrite is employed in the construction of multilayer chip inductors, information storage, biosensors, *etc*[36]. Ni–Cu–Zn ferrite is a soft material that has low magnetic power, good magnetic properties, and high electrical resistance.[37] Recently, much research has been conducted to explore the properties of Ni–Cu–Zn ferrite and develop its applications as a new nanocomposite.[38–42]

The use of carbon nanomaterial composites such as graphene oxide, reduced graphene oxide, carbon nanotubes composites in the recent years have attracted much attention in electrode modification processes due to their suitable properties such as high surface area, conductivity and stability. Also, decrease of the required overpotential of the electrochemical reactions is one of the catalytic properties of hybrids of carbon nanomaterials.[43–46] On the other hand, the application of graphene oxide and graphene-based metal oxide nanocomposites have been widely reported that improved the electrochemical performance.[47] Compared with reduced graphene oxide, graphene oxide/metal oxide hybrid nanocomposites have concerned plentiful attention due to the simple and accessible synthesis method and also the synergistic effect between graphene oxide and metal oxide provide distinctive properties that make them suitable composites for various applications (such as photocatalysts, chemical sensors and biosensors, bioimaging, energy storage and conversion devices, lithium-ion batteries, and fuel cells).[48] In addition to these, magnetic nanoparticles are appropriate materials with graphene oxide hybridization for utilization in electrochemical sensors.[49,50] As mentioned in above, the utilization of magnetic nanoparticles

as electrode surface modifiers has an increasing trend due to the high charge transfer capacity that significantly increases the electron transfer between the analyte and the electrode and consequently improves the sensitivity of electrochemical sensors.[51–55] Despite these advantages, the accumulation of graphene oxide and magnetic nanostructures reduces their efficiency.[56–58] Therefore, to solve this problem, these materials must be dispersed in a porous substrate. Cellulose has all the ideal properties required for sensors and biosensors due to its properties such as inertia, stability and mechanical strength. Cellulose and its derivatives such as carboxymethyl cellulose (CMC) can be used both as membranes and components of nanocomposites. It can also be used as a substrate for stabilizing graphene oxide and ferrite nanoparticles (to prevent them from accumulating on the electrode surface in electrochemical sensors). Hence CMC could act as an excellent option for the upgrade of magnetic nanoparticles composites.[59–65]

As far as we know, the utilization of nickel–copper–zinc ferrite ($Ni_{0.4}Cu_{0.2}Zn_{0.4}Fe_2O_4$) nanocomposite for the determination of OMP (drug) has not been reported in the literature. In this research, the $Ni_{0.4}Cu_{0.2}Zn_{0.4}Fe_2O_4$/CMC/graphene oxide nanosheets (GONs) modified glassy carbon electrode (GCE) as an innovative electrochemical sensor, $Ni_{0.4}Cu_{0.2}Zn_{0.4}Fe_2O_4$/CMC/GONs/GCE, was designed to the determination of OMP. The physicochemical characterization of $Ni_{0.4}Cu_{0.2}Zn_{0.4}Fe_2O_4$/CMC/GONs was examined using spectroscopic and electrochemical techniques [such as scanning electron microscopy (SEM), transmission electron microscopy (TEM), energy-dispersive X-ray spectroscopy (EDX), X-ray diffraction (XRD) and electrochemical impedance spectroscopy (EIS)]. Wonderfully, active sites and synergistic effects (between GONs, CMC and $Ni_{0.4}Cu_{0.2}Zn_{0.4}Fe_2O_4$) of the nanocomposite demonstrated excellently outstanding electrocatalytic performance toward the oxidation of OMP with high sensitivity, long-term stability, desirable selectivity, wide concentration range, and low detection limit. Interestingly, the present developed sensor was able to monitor the OMP concentration in the real samples (pharmaceutical and biological samples).

2. Experimental

2.1. Materials and apparatus

A brief description of chemicals and reagents is presented in the ESI.† Electrochemical measurements were performed by a conventional three-electrode glass cell with a modified glassy carbon electrode (diameter: 3 mm), platinum wire (Pt) and Ag/AgCl (3 M KCl), respectively as the working, auxiliary and reference electrodes in a computer-controlled electrochemical workstation [Autolab, Eco Chemie, Utrecht, the Netherlands and data processing software (GPES, software version 4.7)] at room temperature (20–25 °C). Morphological, surface composition and compositional information of the $Ni_{0.4}Cu_{0.2}Zn_{0.4}Fe_2O_4$/CMC/GONs/GCE were investigated by scanning electron microscopy equipped with X-ray energy dispersive spectroscopy (Phenom prox) and transmission electron microscopy (Carl Ziess AG-Zeiss EM900). X-ray powder diffraction analysis (XRD; D8 Advance Brucker AXS, Karlsruhe, Germany, CuK$_\alpha$ radiation,

$\lambda = 1.5406$ Å) was utilized to characterize the crystal structure of the prepared nanocomposites.

2.2. One-step synthesis of the $Ni_{0.4}Cu_{0.2}Zn_{0.4}Fe_2O_4$/CMC/GONs nanocomposite

An appropriate amount of CMC/GONs composite[66] (ESI†) was dispersed in deionized water and sonicated in an ultrasonic bath and then stirred with a magnetic stirrer for 12 hours. Then appropriate amounts of $NiCl_2 \cdot 6H_2O$, $CuCl_2 \cdot 6H_2O$, $ZnCl_2$, and $FeCl_3 \cdot 6H_2O$ are weighed according to the desired stoichiometry and dissolved in distilled water (as the subsection of 2.2) and added to the dispersed CMC/GONs and sonicated for 1 hour.[67] Then the solution of potassium hydroxide 1 mol L^{-1} was transferred drop by drop to a three-necked flask (in an ultrasonic bath (40 W) at a rate of 10 ml min^{-1} at room temperature) and the pH of the solution was adjusted to 10.5 with ammonia solution.[21,68,69] When the co-precipitation reaction was completed, the sample was kept in a fixed place for 48 hours. The contents of the tube were then centrifuged at 3900 r min^{-1} for 5 minutes and repeated three times. The resulting product was then washed three times with distilled water and dried at 70 °C in an oven for 16 hours. Finally, the product was calcined for 2 hours at 800 °C and then sintered for 2 hours at 900 °C. Other structures of ferrite including single and double metals (M = Ni, Cu, and Zn); $NiFe_2O_4$, $CuFe_2O_4$, $ZnFe_2O_4$ or $Cu_{0.5}Ni_{0.5}Fe_2O_4$, $Cu_{0.5}Zn_{0.5}Fe_2O_4$ and $Ni_{0.5}Zn_{0.5}Fe_2O_4$ were synthesized with the same process by selecting of desired metal salts.

2.3. Preparation of real samples

To evaluate the performance of the $Ni_{0.4}Cu_{0.2}Zn_{0.4}Fe_2O_4$/CMC/GONs/GCE for the electrodetermination of OMP in pharmaceutical tablets and biological samples; their preparation sample procedures are given in detail in the ESI.† Differential pulse voltammetry (DPV) technique and standard addition method were used to determine the OMP in real samples [three times assay of each sample ($n = 3$)].

3. Results and discussion

3.1. Physicochemical characterization of the nanocomposite

Since the morphological and compositional properties of materials play important roles in their physical and chemical properties, the synthesized nanocomposites and modified electrodes were characterized in detail by suitable methods. Typical morphology of nanomaterials were characterized by SEM and obtained results illustrated in Fig. 1 with two magnifications: [A (low), B (high)] GONs, [C (low), D (high)] CMC/GONs, [E (low), F (high)] $Ni_{0.4}Cu_{0.2}Zn_{0.4}Fe_2O_4$ and [G (low), H (high)] $Ni_{0.4}Cu_{0.2}Zn_{0.4}Fe_2O_4$/CMC/GONs. The captured images of A and B exhibit a folding laminar structure with thin sheets for the GONs. The morphology of CMC/GONs (images C and D) is flat and uneven with partially wrinkled structures. Images E and F illustrated the surface morphology of the $Ni_{0.4}Cu_{0.2}Zn_{0.4}Fe_2O_4$. According to these pictures, it is observed that $Ni_{0.4}Cu_{0.2}Zn_{0.4}Fe_2O_4$ nanoparticles are spherical and the particle size distribution is uniform. Also, images G and H in
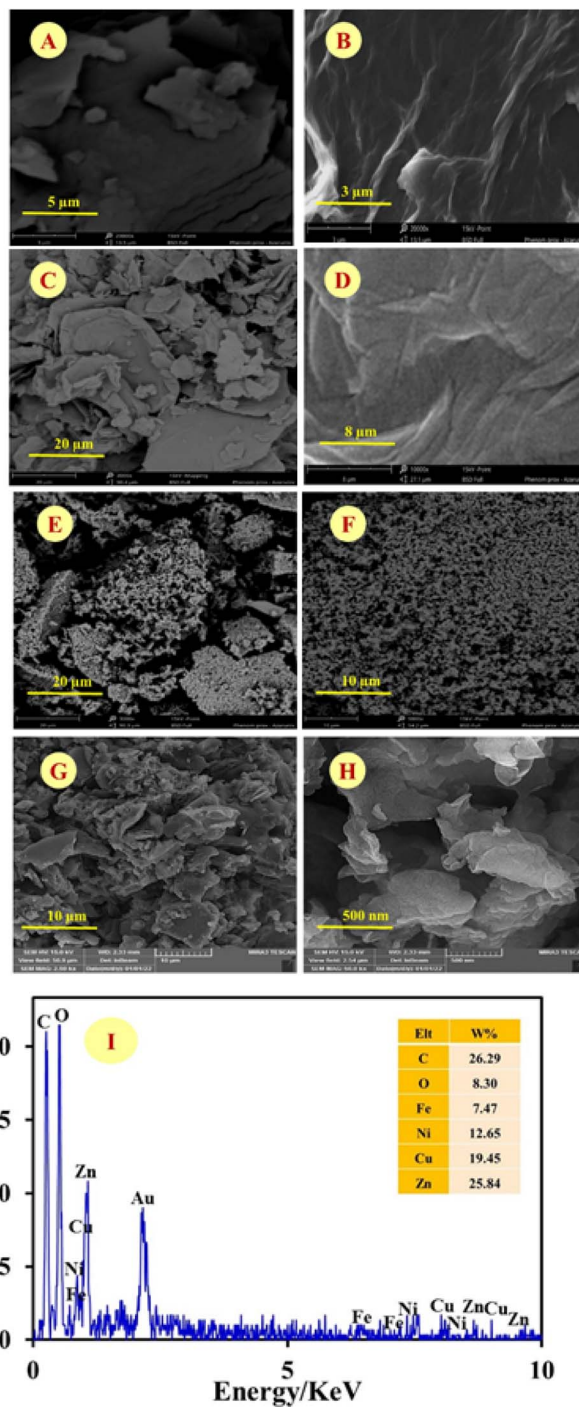

Fig. 1 SEM images with two magnifications of synthesized materials: [A (low), B (high)] GONs, [C (low), D (high)] GONs/CMC, [E (low), F (high)] $Ni_{0.4}Cu_{0.2}Zn_{0.4}Fe_2O_4$, [G (low), H (high)] $Ni_{0.4}Cu_{0.2}Zn_{0.4}Fe_2O_4$/CMC/GONs and (I) the EDX spectrum of as-prepared $Ni_{0.4}Cu_{0.2}Zn_{0.4}Fe_2O_4$/CMC/GONs.

Fig. 1, represents the obtained images for $Ni_{0.4}Cu_{0.2}Zn_{0.4}Fe_2O_4$/CMC/GONs in two magnifications. As can be seen from these images, the accumulated particles are almost regular in shape and the particle size distribution is relatively uniform. Furthermore, the EDX spectrum of $Ni_{0.4}Cu_{0.2}Zn_{0.4}Fe_2O_4$/CMC/GONs clearly reveals the presence of Cu, Ni, Zn, Fe, C, O,
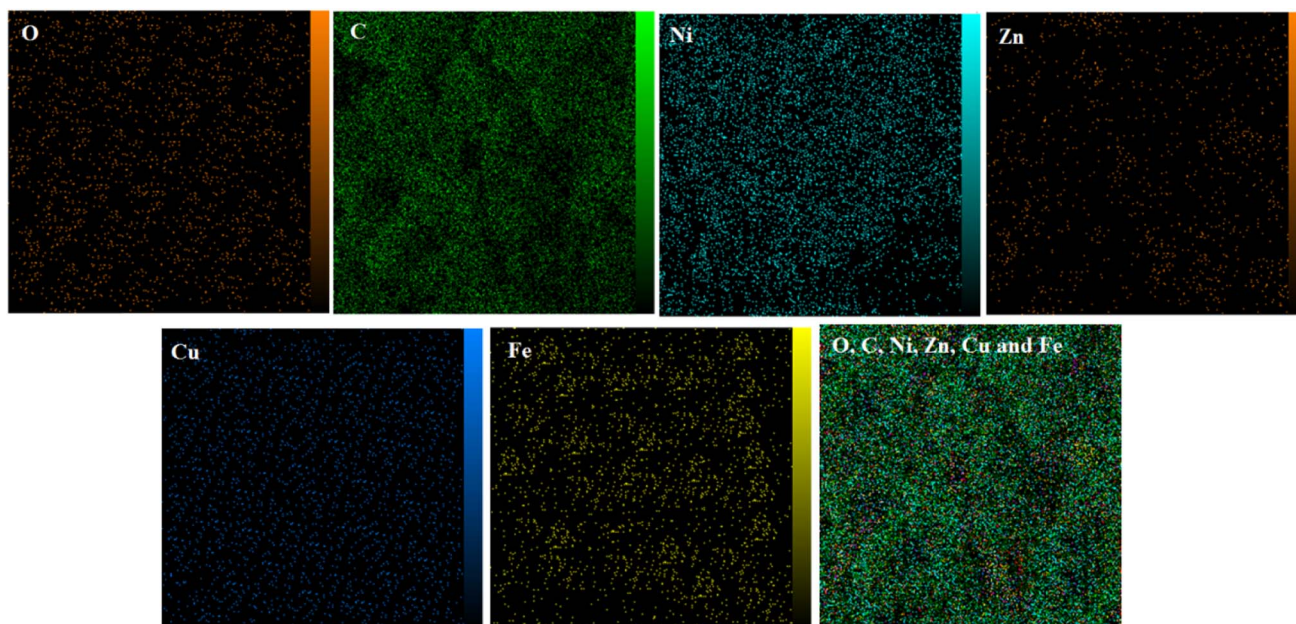
Fig. 2 Elemental mapping of the each atom in the $Ni_{0.4}Cu_{0.2}Zn_{0.4}Fe_2O_4$/CMC/GONs, last map is the distribution of all atoms.

and N elements in the sample (Fig. 1 spectrum I) which signifies the successful synthesis of the $Ni_{0.4}Cu_{0.2}Zn_{0.4}Fe_2O_4$/CMC/GONs nanocomposite. The elemental maps were also recorded to obtain further information about the element distribution of the present atoms. The elemental mapping of the $Ni_{0.4}Cu_{0.2}$-$Zn_{0.4}Fe_2O_4$/CMC/GONs was carried out by EDX analysis and the results were revealed in Fig. 2 which confirms the existence of Fe, Cu, Zn, Ni, C and O atoms with uniform distribution in the synthesized nanocomposite.

Fig. 3 (left) displays the TEM image of the $Ni_{0.4}Cu_{0.2}Zn_{0.4}$-Fe_2O_4/CMC/GONs and reveals that particles are irregular, most likely cubic in shape, and agglomerated. As can be seen from Fig. 3, $Ni_{0.4}Cu_{0.2}Zn_{0.4}Fe_2O_4$/CMC/GONs particle is polygonal, with a size of less than 50 nm, but there are also a few particles with larger size. It is considered that some particles grow abnormally due to incomplete drying process and small amount of water remaining, but most of the particles are normal in size,

proving that the prepared ferrite powder is nanoparticle and nanocrystalline, Fig. 3 (right).

The XRD analysis was used to identify the crystal phase and structural information of freshly prepared GONs, CMC/GONs, $Ni_{0.4}Cu_{0.2}Zn_{0.4}Fe_2O_4$, and $Ni_{0.4}Cu_{0.2}Zn_{0.4}Fe_2O_4$/CMC/GONs nanocomposite (Fig. S1†). In the XRD pattern of GONs (pattern a), the peaks around 2θ equal to 11.09 and 26.4 for reflection (002) of GONs stacked with distances d equal to 6.76 Å and 3.39 Å, respectively, much larger than natural graphite (3.34 Å), which indicates the introduction of oxygen-containing groups on GONs.[65] After loading the GONs with the CMC matrix[66,67] (pattern b), the peak in the GONs almost disappeared on $2\theta = 11.09$, while other diffraction peaks were similar to the peaks of pure GONs.[65] The $Ni_{0.4}Cu_{0.2}Zn_{0.4}Fe_2O_4$ sample (pattern c) shows clear reflections, which can be assigned to (111), (220), (311), (222), (400), (422), (511), and (440) planes that emphasize the successful formation of $Ni_{0.4}Cu_{0.2}Zn_{0.4}Fe_2O_4$ according to
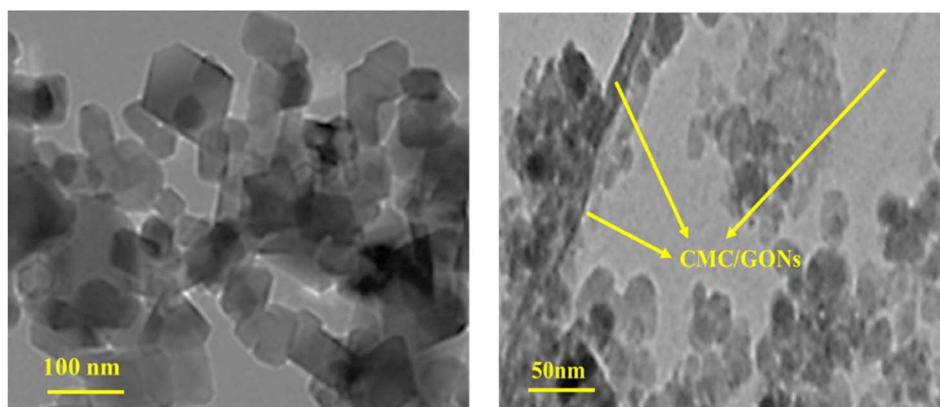

Fig. 3 TEM images of the $Ni_{0.4}Cu_{0.2}Zn_{0.4}Fe_2O_4$/CMC/GONs nanocomposite with different magnification [left (low) and right (high)].

previous research;[68,69] a single phase of $Ni_{0.4}Cu_{0.2}Zn_{0.4}Fe_2O_4$ with cubic spinel structure.[69–71] On the other hand, no extra lines corresponding to any other phases can be detected that indicates the resulting spinel ferrite is relatively pure. In addition, Fig. S1† pattern d depicted the XRD pattern of the $Ni_{0.4}Cu_{0.2}Zn_{0.4}Fe_2O_4$/CMC/GONs. It can be seen that almost all diffraction peaks of $Ni_{0.4}Cu_{0.2}Zn_{0.4}Fe_2O_4$ correspond to the standard pattern of $Ni_{0.4}Cu_{0.2}Zn_{0.4}Fe_2O_4$ nanoparticles presented in the $Ni_{0.4}Cu_{0.2}Zn_{0.4}Fe_2O_4$/CMC/GONs nanocomposite which indicates that the formation of nanocomposite and presence of CMC and GONs has no effect on the crystal structure of ferrite.[72]

Electrochemical characterization of the prepared modified electrode was followed as: electrochemical impedance spectroscopy (EIS) was used to evaluate the interface properties of the modified electrodes compared to the unmodified electrode towards a standard redox system; $[Fe(CN)_6]^{3-}/[Fe(CN)_6]^{4-}$ (5.0 mM) in 0.1 M KCl solution. As shown in Fig. 4A (Nyquist plots), the charge transfer resistance (R_{ct}) is estimated to be 309.83, 235.03, 192.45, 176.08, and 128.32 $\Omega.cm^2$ for GCE, GONs/GCE,

Fig. 4 (A) Nyquist plots of the unmodified GCE (a), GONs/GCE (b), CMC/GONs/GCE (c), $Ni_{0.4}Cu_{0.2}Zn_{0.4}Fe_2O_4$/GCE (d) and $Ni_{0.4}Cu_{0.2}Zn_{0.4}Fe_2O_4$/CMC/GONs/GCE (e) in 0.1 M KCl containing 5 mM $[Fe(CN)_6]^{3-}/[Fe(CN)_6]^{4-}$ as the redox probe. (B) CVs of the same electrodes in similar conditions.

Table 1 The R_{ct} value of different electrodes

Electrode	R_{ct}
$Ni_{0.4}Cu_{0.2}Zn_{0.4}Fe_2O_4$/CMC/GONs/GCE	128.32
$Ni_{0.4}Cu_{0.2}Zn_{0.4}Fe_2O_4$/GCE	176.08
CMC/GONs/GCE	192.45
GONs/GCE	235.03
GCE	309.83

CMC/GONs/GCE, $Ni_{0.4}Cu_{0.2}Zn_{0.4}Fe_2O_4$/GCE and $Ni_{0.4}Cu_{0.2}Zn_{0.4}Fe_2O_4$/CMC/GONs/GCE, respectively (as shown in Table 1). According to the results, it can be seen that the $Ni_{0.4}Cu_{0.2}Zn_{0.4}Fe_2O_4$/CMC/GONs/GCE shows a smaller distinct semicircular arc with a low R_{ct} value compared to other step-by-step modified electrodes which indicates that the $Ni_{0.4}Cu_{0.2}Zn_{0.4}Fe_2O_4$/CMC/GONs can improves the charge-transfer kinetics and implicates the excellent electrocatalytic activity of the designed nanocomposite. Furthermore, the inset of Fig. 4B displays the equivalent circuit model for $Ni_{0.4}Cu_{0.2}Zn_{0.4}Fe_2O_4$/CMC/GONs/GCE, which is consistent with the results of the corresponding Nyquist plots and mirror electron shifting characteristics $[Fe(CN)_6]^{3-}/[Fe(CN)_6]^{4-}$ redox probe.[21]

The electrochemical responses of the prepared electrodes in redox probe solution, $Fe(CN)_6^{3-}/Fe(CN)_6^{4-}$ (5.0 mM) and KCl (0.1 M), were also recorded by the cyclic voltammetric method. Fig. 4B shows the obtained cyclic voltammograms for GCE (curve a), GONs/GCE (curve b), CMC/GONs/GCE (curve c), $Ni_{0.4}Cu_{0.2}Zn_{0.4}Fe_2O_4$/GCE (curve d), and $Ni_{0.4}Cu_{0.2}Zn_{0.4}Fe_2O_4$/CMC/GONs/GCE (curve e). From these results, the real surface area of the modified electrodes was determined based on the plots of the acodic peak current *versus* square root of scan rate (not shown here) and the Randles–Sevick formula (eqn (1)):[73–76]

$$I_p = 2.69 \times 10^5 n^{3/2} A C_0 D^{1/2} v^{1/2} \qquad (1)$$

In eqn (1), I_p, n, A, C, D, and V are the anodic peak current, the number of electrons in the reaction ($n = 1$), electrochemical real surface area, electroactive species concentration (5.0 mM), the diffusion coefficient of $[Fe(CN)_6]^{3-}/[Fe(CN)_6]^{4-}$ (7.6×10^{-6} cm^2 s^{-1}),[75,77] and the scan rate, respectively. Based on the calculation, the real surface areas were found as: 0.023, 0.048, 0.083, 0.284, and 0.686 cm^2 for GCE, GONs/GCE, CMC/GONs/GCE, $Ni_{0.4}Cu_{0.2}Zn_{0.4}Fe_2O_4$/GCE, and $Ni_{0.4}Cu_{0.2}Zn_{0.4}Fe_2O_4$/CMC/GONs/GCE, respectively.

3.2. Electrocatalysis performance of the $Ni_{0.4}Cu_{0.2}Zn_{0.4}Fe_2O_4$/CMC/GONs/GCE towards OMP oxidation

In order to evaluate the electrocatalysis performance of the $Ni_{0.4}Cu_{0.2}Zn_{0.4}Fe_2O_4$/CMC/GONs/GCE towards the oxidation of OMP, the cyclic voltammetric method was utilized in phosphate buffer solution (PBS, pH = 6.0) at the potential window from 300 to 1100 mV s^{-1} *vs.* Ag/AgCl in the presence of OMP (25 μM) with a fixed scan rate at 100 mVs^{-1}. The obtained results in these condition at the unmodified GCE, GONs/GCE, CMC/GONs/GCE, $Ni_{0.4}Cu_{0.2}Zn_{0.4}Fe_2O_4$/GCE and $Ni_{0.4}Cu_{0.2}Zn_{0.4}Fe_2$-$O_4$/CMC/GONs/GCE were shown in Fig. 5A. As shown, at the

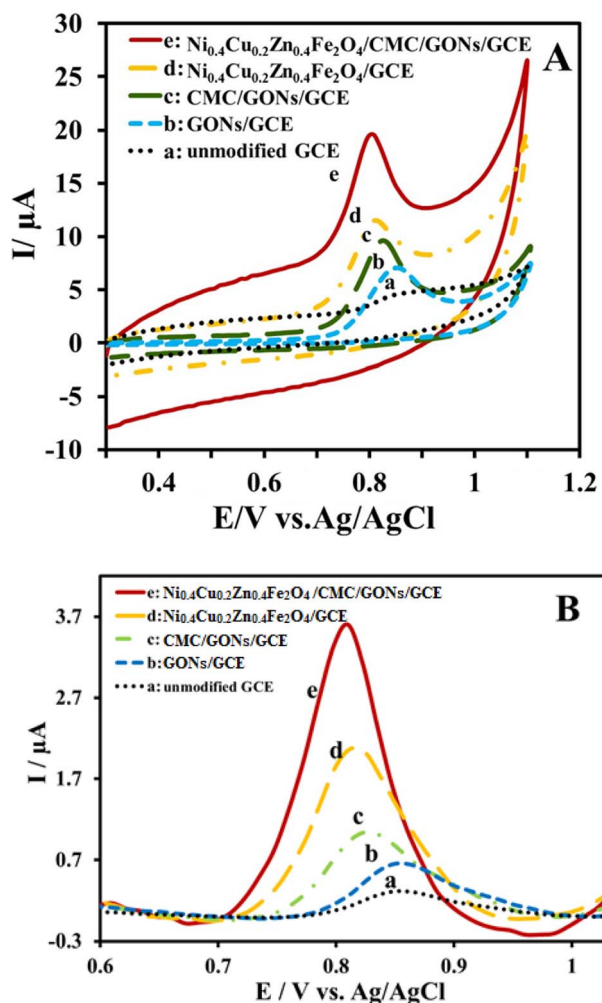Fig. 5 (A) CVs and (B) DPVs of the OMP at different electrodes: unmodified GCE (a), GONs/GCE (b), CMC/GONs/GCE (c), and $Ni_{0.4}$-$Cu_{0.2}Zn_{0.4}Fe_2O_4$/GCE (d), and $Ni_{0.4}Cu_{0.2}Zn_{0.4}Fe_2O_4$/CMC/GONs/GCE (e). Cyclic voltammetric conditions: scan rate of 100 mVs^{-1} for 25 μM OMP in pH 6.0 PBS (0.1 M). DPV conditions: pulse amplitude 0.05 V, scan rate 0.025 V s^{-1} and pulse time 0.04 s for 4 μM OMP in pH 6.0 PBS phosphate buffer (0.1 M).

contributions of CMC, GON and $Ni_{0.4}Cu_{0.2}Zn_{0.4}Fe_2O_4$ which increase the electrocatalytic performances of the $Ni_{0.4}Cu_{0.2}$-$Zn_{0.4}Fe_2O_4$/CMC/GONs/GCE. On the other hand, high electrocatalysis activity of the $Ni_{0.4}Cu_{0.2}Zn_{0.4}Fe_2O_4$/CMC/GONs/GCE may be attributable to the synergistic effects of these components, the effective interaction of $Ni_{0.4}Cu_{0.2}Zn_{0.4}Fe_2O_4$ nanoparticles with OMP molecules[78] on the electrode surface and the catalytic effect of the nanocomposite, $Ni_{0.4}Cu_{0.2}Zn_{0.4}Fe_2O_4$/CMC/GONs/GCE (Fig. 3A curve a) in analogy with CMC/GONs/GCE (Fig. 5A curve c).[21] Actually, the excellent increase in the anodic peak current and decrease in the peak potential of OMP oxidation implies that the modified $Ni_{0.4}Cu_{0.2}Zn_{0.4}Fe_2O_4$/CMC/GONs/GCE accelerates the rate of electron transfer reaction. Finally, as can be seen, no cathodic peak is observed for OMP electroreaction during the reverse scan, it can be concluded that the electrochemical reaction of OMP at the $Ni_{0.4}Cu_{0.2}Zn_{0.4}Fe_2$-$O_4$/CMC/GONs/GCE is totally irreversible based on scientific findings.[79]

Also, the DPVs were recorded in 4 μM OMP on the surface of unmodified GCE, GONs/GCE, CMC/GONs/GCE, $Ni_{0.4}Cu_{0.2}$-$Zn_{0.4}Fe_2O_4$/GCE and $Ni_{0.4}Cu_{0.2}Zn_{0.4}Fe_2O_4$/CMC/GONs/GCE and shown in Fig. 5B. As can be seen, at the surface of unmodified GCE, in the scanning potential window of 0.6 to 1.0 V, a very weak and broad anodic peak current (curve a) was observed for OMP oxidation due to slow electron transfer.[21] In addition, the peak current of OMP electrooxidation improved at the GONs/GCE (curve b) and significantly increased at the surface of the CMC/GONs/GCE (curve c). The $Ni_{0.4}Cu_{0.2}Zn_{0.4}Fe_2O_4$/GCE shows a noteworthy high current for OMP oxidation (curve d). While, at the $Ni_{0.4}Cu_{0.2}Zn_{0.4}Fe_2O_4$/CMC/GONs/GCE (curve e) for OMP oxidation, a clear and sharp oxidation peak with the highest peak current is observed, which indicates an improvement in sensitivity in the determination process of OMP due to the excellent electronic conductivity of the nanocomposite and the high electroactive surface of the $Ni_{0.4}Cu_{0.2}Zn_{0.4}Fe_2O_4$/CMC/GONs/GCE. As can be seen, the DPVs results are in good agreement with the results of the cyclic voltammetric method.

unmodified GCE (curve a), a very low redox current signal for OMP oxidation was obtained ($I_p = 0.95$ μA, $E_p = 0.898$ V). While others electrodes show high oxidation peaks: GONs/GCE ($I_p = 4.15$ μA, $E_p = 0.844$ V), CMC/GONs/GCE ($I_p = 6.23$ μA, $E_p = 0.813$ V), $Ni_{0.4}Cu_{0.2}Zn_{0.4}Fe_2O_4$/GCE ($I_p = 7.73$ μA, $E_p = 0.797$ V), and $Ni_{0.4}Cu_{0.2}Zn_{0.4}Fe_2O_4$/CMC/GONs/GCE ($I_p = 11.24$ μA, $E_p = 0.787$ V). As depicted in Fig. 5A, the $Ni_{0.4}Cu_{0.2}Zn_{0.4}Fe_2O_4$/CMC/GONs/GCE (curve e) gives a well-defined peak for OMP oxidation with highest peak current and lower potential compared to all the modified GCEs.

These results indicate that the electrooxidation process of OMP at the $Ni_{0.4}Cu_{0.2}Zn_{0.4}Fe_2O_4$/CMC/GONs/GCE surface is significantly increases due to the simultaneous presence of the GONs, CMC and ferrite nanoparticles in the nanocomposite, which has good conductivity from that of GONs, high specific surface from that of CMC and ferrite and synergistic

3.3. Optimization of various experimental factors

Some important and key factors on the reaction rate and signal intensity including the amount and chemical structure of modifier, effect of pH, scan rate and accumulation time in the electrocatalysis process were studied and optimized.[80,81] Since the amount of modifier plays an essential role in OMP electrocatalysis, different amounts of modifier were examined by linear sweep voltammetry (LSV) method in the electrode modification process (0.5 mg ml^{-1} to 3 mg ml^{-1}) (Fig. 6A). The results (inset of Fig. 6A) show that the modified electrode with 1 mg ml^{-1} of modifier provides a significant high current signal compared to higher modifier values, while a further increase of the modifier reduces peak current. This behavior may be attributed to the fact that amounts higher than 1 mg ml^{-1} cause roughness on the surface, resulting in flattened noses and reduced sensitivity. Hence, the amount of 1 mg ml^{-1} was chosen as the optimal value for subsequent experimental tests in OMP electrocatalysis.
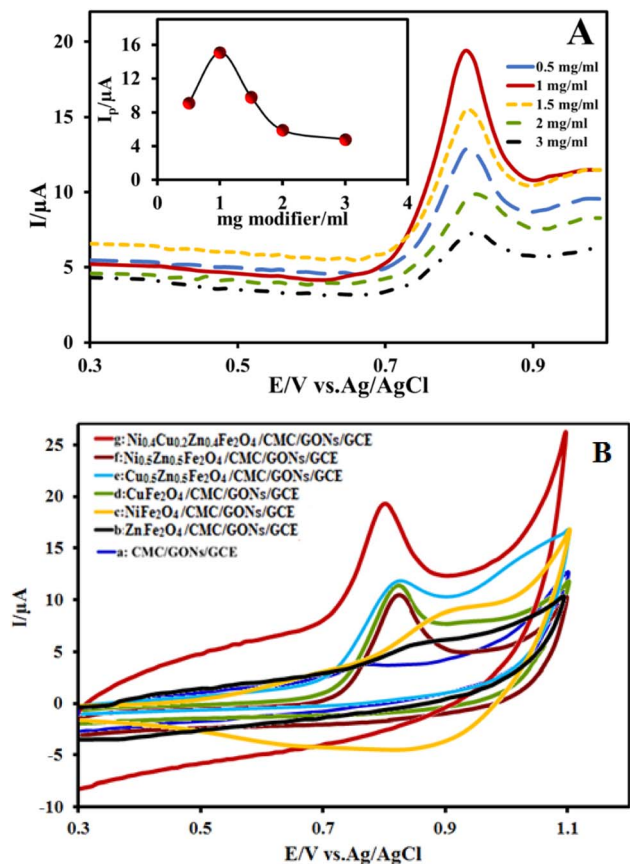
Fig. 6 (A) LSVs of the $Ni_{0.4}Cu_{0.2}Zn_{0.4}Fe_2O_4$/CMC/GONs/GCE at various amounts of modifier in PBS (0.1 M, pH 6.0) in a solution containing 25 μM OMP (inset is I_p vs. amount of modifier). (B) CVs of the OMP at different electrodes: CMC/GONs/GCE (a), $ZnFe_2O_4$/CMC/GONs/GCE (b), $NiFe_2O_4$/CMC/GONs/GCE (c), $CuFe_2O_4$/CMC/GONs/GCE (d) and $Cu_{0.5}Zn_{0.5}Fe_2O_4$/GCE (e), $Ni_{0.5}Zn_{0.5}Fe_2O_4$/GCE (f) and $Ni_{0.5}Cu_{0.5}Fe_2O_4$/CMC/GONs/GCE (e). Cyclic voltammetric conditions: scan rate of 100 mV s^{-1} for 25 μM OMP in pH 6.0 PBS (0.1 M).

The chemical structure of synthesized ferrite nanoparticles as a part of nanocomposite modifier can also affect the signal of OMP electrooxidation due to the synergistic contribution of metals. Therefore, in order to study of effect of each metal in the ferrite structure on the electrocatalysis activity, different structures of ferrite including single, double, and triple metals (M = Ni, Cu and Zn) involved in ferrite components were synthesized and used as modifier in the OMP oxidation. The obtained cyclic voltammograms related to different nanocomposite modifiers are shown in Fig. 6B. As seen before (Fig. 5 curve c), the voltammogram related to CMC/GONs/GCE shows a very weak electrocatalysis response to the OMP oxidation with lowest peak current value. Comparing this voltammogram with the voltammograms of Fig. 6B shows that by adding the ferrite nanoparticles to the CMC/GONs system, the peak current value of the OMP oxidation increases, which indicates its positive effect on the anodic peak current. The plot of $ZnFe_2O_4$/CMC/GONs/GCE gave approximately 2 times higher peak current values than the CMC/GONs/GCE at the same concentration of OMP. It was also observed that the modifier containing $NiFe_2O_4$/CMC/

GONs/GCE showed approximately 3 times the peak current values, while the nanocomposite containing $CuFe_2O_4$/CMC/GONs/GCE showed approximately 4 times the peak current values. Also, the voltammograms of double ferrites; $Cu_{0.5}Zn_{0.5}Fe_2O_4$/CMC/GONs/GCE and $Ni_{0.5}Zn_{0.5}Fe_2O_4$/CMC/GONs/GCE were examined. Of these two the $Cu_{0.5}Zn_{0.5}Fe_2O_4$/CMC/GONs/GCE shows high electrocatalysis activity. Finally, the triple metal ferrites; $Ni_{0.4}Cu_{0.2}Zn_{0.4}Fe_2O_4$, show the highest peak current in the OMP oxidation due to the synergistic contribution of metals.

Another effective parameter that must be optimized is the pH of the solution in the electrooxidation of OMP. For this purpose, the effect of pH on the oxidation of OMP at the $Ni_{0.4}$-$Cu_{0.2}Zn_{0.4}Fe_2O_4$/CMC/GONs/GCE was studied by CV technique for 10 ml 0.1 M PBS containing 25 μM OMP with different pH values in the range of 3.0 to 9.0 (Fig. S2†) at the scan rate of 100 mV s^{-1}. The results illustrated that the pH value affects both the peak current and peak potential of OMP oxidation. As can be seen, the anodic peak current increased with the pH change (inset A) from 3.0 to 6.0 and then decreased (in pH from pH 7.0 to 9.0). Also, the oxidation peak potential of OMP shifts to a negative potential with increasing pH under a regression equation of $E_{pa}(V) = -0.0529$ pH $+ 1.1388$ ($R^2 = 0.9923$). The peak potential diagram in terms of pH can be seen in inset B of Fig. S2.† As shown, the slope of the peak potential changes is 0.0529 V pH^{-1} (obtained as a function of the pH of the solution), which is close to the slope of the Nernst equation.[21,82] Therefore, we can deduce that the number of electrons and protons involved in the oxidation reaction are equal. Based on the obtained results and according to the literature reported for OMP oxidation, the suggested electrooxidation mechanism of OMP can be expressed as Scheme S2,† in which the number of electrons and protons is 1.[21,22,83,84] From the chemical point, OMP is a weak lipophilic base with $pK_{a1} = 4.2$ and $pK_{a2} = 9$ and decomposes unless protected against acidic conditions.[85,86] Based on the values of pK_a for OMP, at the pHs lower than the pK_{a1}, due to the protonation of OMP molecule, its oxidation process may be more difficult and therefore the current should increase with increasing pH around its pK_{a1}. At pH values above 9.0, the slope changes and the peak potential is independent of pH. Due to the propinquity of the intersection point of the curve to the pK_{a2} value of benzimidazole moiety present in the OMP molecule (about 8.6), it is assumed that the oxidation of OMP is related to the removal of a proton from the imidazole part of the OMP molecule in the oxidation of this molecule.[87] This result is consistent with the electrochemical oxidation mechanism of OMP that shown in Scheme S2†.[83,84] On the other hand, the electrochemical oxidation mechanism of OMP involves the removal of an electron and the formation of an intermediate cation radical. Then deprotonation occurs, after which the radical cation reacts with water molecules and finally leads to the production of an irreversible hydroxylated product.[88,89] Due to the excellent response of the obtained sensor in buffer solution at pH = 6.0, OMP oxidation has the best and highest signal at pH = 6.0, this pH was used in subsequent experiments which is favorable for determining the OMP in real biological conditions.

To obtain more detailed information about the kinetic and the nature of the OMP electrooxidation process at the $Ni_{0.4}$-$Cu_{0.2}Zn_{0.4}Fe_2O_4$/CMC/GONs/GCE, the effect of the potential sweep rate by employing the several scan rates from 10–120 mVs^{-1} on the peak current response was evaluated by CV analysis in the 0.1 M PBS (pH = 6.0) and 25 μM of OMP (Fig. S3†). As can be seen from Fig. S3,† the analysis of anodic peak current in terms of scan rate (inset A) shows a linear relationship between peak current (I_P) and scan rate (v) with linear equation; I (μA) = 0.9789 + 0.1134v (v in mV s^{-1}), (R^2 = 0.9903), which indicates that the electrode reaction process is an adsorption-controlled process.[21,90] Also, by plotting the log peak current (I_p) in terms of the log of scan rate (inset B), a linear graph was obtained with a slope of 0.8919 [log I_p (μA) = 0.8919 log v (mV s^{-1}) − 0.687 (R^2 = 0.9955)]. The obtained value is theoretically close to 1.0 for reactions that are classified as adsorption-controlled processes.[22]

Furthermore, based on the theory of Laviron for an irreversible electrode process and the E-Log v plot (Fig. S4†), and following equation (eqn (2)),[91] the catalytic rate constant (k_s) and the values of electron transfer coefficients (α_n) of OMP electrooxidation were calculated at the $Ni_{0.4}Cu_{0.2}Zn_{0.4}Fe_2O_4$/CMC/GONs/GCE.

$$E_p = E^{\circ\prime} + \left(\frac{2.303RT}{\alpha_n F}\right)\log\left(\frac{RTk_s}{\alpha_n F}\right) + \left(\frac{2.303RT}{\alpha_n F}\right)\log v \quad (2)$$

where n, F, R, T and other symbols have their conventional and usual meanings. By using the Laviron equation, the α_n and K_s (catalytic constant) were calculated to be about 0.47 and 1.31 s^{-1}, respectively.

Optimization of accumulation time is very important in conditions where the proposed reaction mechanism is the adsorption process. Because, this factor can affect the amount of OMP accumulated on the modified electrode surface. Fig. S5† depicts the diagram of the anodic peak current in terms of the accumulation time for the 4 μM OMP solution under optimal conditions in the range of 10–70 s by DPV technique, where a linear relationship between anodic peak current and time was observed. The I_{pa} value increased rapidly with increasing preconcentration time and reached an uppermost value at 50 s, while the peak current remained constant with a further increase in accumulation time. Therefore, in the following experiments, the optimal accumulation time was selected as 50 s.

3.4. Electrochemical determination of OMP

Due to various advantages; higher current sensitivity, lower background currents, better performance and more acceptable peak resolutions, the DPV technique was used to quantitate the OMP by the proposed electrode; $Ni_{0.4}Cu_{0.2}Zn_{0.4}Fe_2O_4$/CMC/GONs/GCE. To achieve the working range of newly designed sensor; $Ni_{0.4}Cu_{0.2}Zn_{0.4}Fe_2O_4$/CMC/GONs/GCE, the corresponding DPV profiles at different concentrations of OMP were recorded under optimized conditions (0.1 M PBS at pH = 6.0). Fig. 7 shows DPVs grams of the OMP in different concentration ranges.
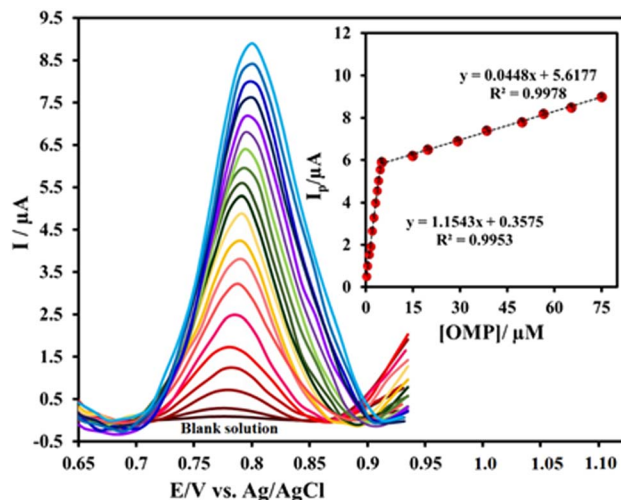
Fig. 7 DPVs of $Ni_{0.4}Cu_{0.2}Zn_{0.4}Fe_2O_4$/CMC/GONs/GCE in the absence (blank solution) and presence of 0.24–75 μM OMP in 0.1 M PBS phosphate buffer (pH = 6.0). Inset: the related linear relationships between the I_p and OMP concentrations (calibration curve) in the ranges of 0.24–5 and 5–75 μM.

The linear response were obtained for the OMP in the ranges of 0.24–5 μM and 5–75 μM with linear equations: I_p = 1.1543 [OMP] + 0.3575 and I_p = 0.0448 [OMP] + 5.6177 and correlation coefficient of R^2 = 0.9953 and R^2 = 0.9978 (inset), respectively. The calculated limit of detection (LOD) and limit of quantitation (LOQ) (LOD = 3S m^{-1} and LOQ = 10S m^{-1}, where S = standard deviation and m = slope of the calibration curve)[92] are 0.22 ± 0.05 μM and 0.73 ± 0.05 μM, respectively, suggesting that the proposed sensor can detect the low concentrations of OMP. In summary, the comparison of the results obtained from the present designed sensor with other OMP electrochemical sensors reported in the literature shows that the strategy applied in this study in terms of detection limit and dynamic range is well comparable with previous reports or better than the provided methods (as clearly shown in Table 2). The results show the high and acceptable performance of the present sensor for the determination of OMP by the DPV method.

3.5. Interference studies

Anti-interference capability is one of the important indicators to evaluate the practical application of a sensor. In interference study, the interferer species are usually selected that have oxidation or reduction behavior near to the main analyte or presented in the analyte matrix (real samples). Therefore, the responses of the $Ni_{0.4}Cu_{0.2}Zn_{0.4}Fe_2O_4$/CMC/GONs/GCE was investigated for the some selected interferences in determination of 4 μM OMP on behalf of common mineral ions (K^+, Na^+, Zn^{2+}, Mg^{2+}, Ca^{2+}, Fe^{2+} and Cu^{2+}) and also biological compounds (glucose, sucrose, ascorbic acid, citric acid, and uric acid) with a 10-folds concentrations higher than OMP under optimal experimental conditions (0.1 M PBS, pH = 6) and measured peak currents in DPV technique shown in Fig. S6.† According to the results, it is obvious that there is no noticeable and significant change in the OMP signal, which indicates that the

Table 2 Comparison of analytical parameters of OMP determination at the $Ni_{0.4}Cu_{0.2}Zn_{0.4}Fe_2O_4$/CMC/GONs/GCE with other modified electrodes[a]

Electrode	Method	Linear range (μM)	LOD (μM)	Sample	Ref.
Mercury electrode	DPV	0.07–300	0.02	Drug, serum	13
$Ni_{0.5}Zn_{0.5}Fe_2O_4$/Gr/GCE	DPV	0.02–1.4	0.13	Drug, serum	22
BDDE	DPV	2.3–14	0.91	Urine, drug	23
Mercapto-NP-F-CPE	DPV	0.00025–25.0	0.095	Urine, plasma, water, drug	83
EPG	SWV	0.11–100	0.019	Drug, serum	87
CuO NPs/CPE	ALSV	0.1–2	0.013	Drug, serum	91
CPE	SWV	0.2–50	0.025	Drug	93
GCE	DPV	2.9–58	0.55	Drug	94
S-MWCNTs-Fe_3O_4/PPDA/GCE	LSV	0.05–9.0	0.015	Urine, plasma, water, drug	95
NiOxNPs/GCE	AP	4.5–120	0.4	Drug	96
Poly (alizarin)/GCE	DPV	400–1000	0.715	Drug	97
DME	DPP	0.1–1	0.7	Drug, serum	98
Chit-S@gC_3N_4/GCE	DPV	0.6–260	0.02	Drug, serum, urine	99
$Ni_{0.4}Cu_{0.2}Zn_{0.4}Fe_2O_4$/CMC/GONs/GCE	DPV	0.24–5 5–75	0.22	Drug, serum	This work

[a] LOD: detection of limit; DPV: differential pulse voltammetry; SWV: square wave voltammetry; DPP: differential pulse polarography; AP: amperometry; LSV: linear sweep voltammograms; GCE: glass carbon electrode; CPE: carbon paste electrode; BDDE: boron-doped diamond electrode; DME: dropping mercury electrode; EPG: edge-plane pyrolytic graphite electrode; NiOxNPs: nickel oxide nanoparticles.

Table 3 Results of recovery test of OMP in real samples ($n = 3$)

No.	Added (μM)	Found (μM)	Recovery (%)	RSD%
Human serum	0.00	Not detected	—	—
	2	2.01	100.50	2.88
	5	4.98	99.60	3.15
	10	9.88	98.80	3.36
Omeprazol tablet	0.00	19.36	—	3.05
	2	21.16	99.06	3.42
	3	22.43	100.31	2.65
	4	22.95	98.24	3.13

proposed sensor is selective and suitable for determining OMP in complicated matrices.

3.6. Analytical applications of the $Ni_{0.4}Cu_{0.2}Zn_{0.4}Fe_2O_4$/CMC/GONs/GCE in real samples

To evaluate the analytical and actual application of the newly designed sensor, OMP was determined in real samples (tablet and human serum) under optimal conditions by DPV technique, and the obtained results are listed in Table 3. The sample preparation of the real samples was described in the experimental section (ESI†). The obtained recovery range values of the human blood serum (98.80–100.50%) and tablet samples (98.24–100.31%) with low RSDs (2.88% for human blood serum and 2.65% for tablet samples) are acceptable. Therefore, it can be concluded that the proposed nanocomposite-modified electrode has significant potential that can be used to detect the OMP in real samples with a good recovery range.

4. Conclusion

This work summarizes the synthesis of $Ni_{0.4}Cu_{0.2}Zn_{0.4}Fe_2O_4$/CMC/GONs nanocomposite through a one-step, sustainable and rapid method. The synthesized nanocomposite was characterized by different suitable techniques including SEM, TEM, XRD, EDX and EIS. In the next step, the GCE was modified by the obtained nanocomposite, $Ni_{0.4}Cu_{0.2}Zn_{0.4}Fe_2O_4$/CMC/GONs/GCE, and then was used to the electrooxidation of OMP. The results show that the obtained modified electrode has excellent electrocatalytic activity for OMP oxidation in low positive potential (0.797 V) due to more active sites, large surface area, high conductivity, synergistic effects and fast electron transfer. The experimentally results display that the newly designed sensor has excellent analytical performance for OMP detection; wide working range (0.24–5 and 5–75 μM), low LOD (0.22 ± 0.05 μM) and LOQ (0.73 ± 0.05 μM), good sensitivity (1.1543 μA $μM^{-1}$ cm^{-2}), long-term stability, acceptable selectivity, and high reproducibility. The use of the designed sensor to determination of OMP in real samples such as human blood serum and OMP tablets demonstrates that its appreciable sensing potential in complex matrices. So, the prepared sensor could certainly be a promising candidate for a wide range of electrochemical and bioassay applications.

Conflicts of interest

There are no conflicts to declare.

Acknowledgements

References

1 K. Jana, T. Bandyopadhyay and B. Ganguly, Stereoselective Metabolism of omeprazole by cytochrome P450 2C19 and 3A4: Mechanistic Insights from DFT Study, *J. Phys. Chem. B*, 2018, **122**(22), 5765–5775.

2 A. O. El-Nezhawy, A. R. Biuomy, F. S. Hassan, A. K. Ismaiel and H. A. Omar, Design, synthesis and pharmacological

evaluation of omeprazole-like agents with anti-inflammatory activity, *Bioorg. Med. Chem.*, 2013, **21**(7), 1661–1670.

3 E. Cheng, Proton Pump Inhibitors for Eosinophilic Esophagitis, *Curr. Opin. Gastroenterol.*, 2013, **29**(4), 416–420.

4 D. Lopes-de-Campos, C. Pereira-Leite, P. Fontaine, A. Coutinho, M. Prieto, B. Sarmento, S. Jakobtorweihen, C. Nunes and S. Reis, Interface-Mediated Mechanism of Action-The Root of the Cytoprotective Effect of Immediate-Release Omeprazole, *J. Med. Chem.*, 2021, **64**(8), 5171–5184.

5 D. S. Strand, D. Kim and D. A. Peura, 25 years of proton pump inhibitors: a comprehensive review, *Gut Liver*, 2017, **11**(1), 27–37.

6 D. Šahnić, E. Meštrović, T. Jednačak, I. Habinovec, J. Parlov Vuković and P. Novak, Monitoring and quantification of omeprazole synthesis reaction by in-line Raman spectroscopy and characterization of the reaction components, *Org. Process Res. Dev.*, 2016, **20**(12), 2092–2099.

7 M. S. Elmasry, W. S. Hassan, M. Y. El-Mammli and M. Badrawy, Earth friendly spectrophotometric methods based on different manipulation approaches for simultaneous determination of aspirin and omeprazole in binary mixture and pharmaceutical dosage form: Comparative statistical study, *Spectrochim. Acta, Part A*, 2022, **266**, 120436.

8 J. J. B. Nevado, G. C. Peñalvo, R. M. R. Dorado and V. R. Robledo, Simultaneous determination of omeprazole and their main metabolites in human urine samples by capillary electrophoresis using electrospray ionization-mass spectrometry detection, *J. Pharm. Biomed. Anal.*, 2014, **92**, 211–219.

9 H. M. Lotfy, M. A. Hegazy, S. Mowaka and E. H. Mohamed, Validated spectrophotometric methods for simultaneous determination of Omeprazole, Tinidazole and Doxycycline in their ternary mixture, *Spectrochim. Acta, Part A*, 2016, **153**, 321–332.

10 M. S. Elmasry, A. Serag, W. S. Hassan, Ma. Y. El-Mammli and M. Badrawy, Spectrophotometric determination of aspirin and omeprazole in the presence of salicylic acid as a degradation product: a comparative evaluation of different univariate/multivariate post processing algorithms, *J. AOAC Int.*, 2022, **105**(1), 309–316.

11 I. A. Alamin and A. A. Elbashir, A new study on Omeprazole spectrophotometric determination using 9-Fluorenyl methyl chloroformate as derivatizing agent, *J. anal. pharm. res.*, 2019, **8**(2), 38–43.

12 G. Hancu, L. A. Papp and A. Rusu, Chiral Separation of the Enantiomers of Omeprazole and Pantoprazole by Capillary Electrophoresis, *Chromatographia*, 2015, **78**, 279–284.

13 S. Beheshti, H. Ahmad Panahi and A. Feizbakhsh, Development of Thermo-Sensitive and Magnetic Molecularly Imprinted Polymer for Extraction of Omeprazole in Biological and Pharmaceutical Samples Coupled by High Performance Liquid Chromatography, *ChemistrySelect*, 2023, **8**(10), e202203237.

14 M. Rambla-Alegre, J. Esteve-Romero and S. Carda-Broch, Analysis of omeprazole and its main metabolites by liquid chromatography using hybrid micellar mobile phases, *Anal. Chim. Acta*, 2009, **633**(2), 250–256.

15 G. Yenduri and S. Navuluri, Analytical high performance liquid chromatography method for estimating the combination of aspirin and omeprazole in bulk and tablet dosage form, *Marmara Pharm. J.*, 2018, **22**(4), 502–510.

16 E. Johansson and A. Karlsson, Jufang Wu Ludvigsson Ultra high performance liquid chromatography method development for separation of omeprazole and related substances on core-shell columns using a Quality by Design approach, *J. Sep. Sci.*, 2020, **43**(4), 696–707.

17 A. M. Kashid and O. H. Kolhe, Simultaneous Densitometric Determination of Aspirin and Omeprazole by High-Performance Thin-Layer Chromatography, *J. Planar Chromatogr. - Mod. TLC*, 2019, **32**(6), 501–504.

18 B. Mostafiz, L. Fotouhi and P. Seyed Dorraji, An electrochemical sensor based on an Eriochrome Black T polymer and deep eutectic solvent for the simultaneous determination of omeprazole and lansoprazole, *Anal. Methods*, 2020, **12**, 4072–4079.

19 K. Pandian, J. Kalayarasi and S. C. Gopinath, Metal-free Sulfur-doped graphitic carbon nitride-modified GCE-based electrocatalyst for the enhanced electrochemical determination of omeprazole in Drug formulations and Biological Samples, *Biotechnol. Appl. Biochem.*, 2022, **69**, 2766–2779.

20 J. S. Stefano, T. F. Tormin, J. P. da Silva, E. M. Richter and R. A. Munoz, Amperometric determination of omeprazole on screen-printed electrodes using batch injection analysis, *Microchem. J.*, 2017, **133**, 398–403.

21 A. Afkhami, A. Bahiraei and T. Madrakian, Application of nickel zinc ferrite/graphene nanocomposite as a modifier for fabrication of a sensitive electrochemical sensor for determination of omeprazole in real samples, *J. Colloid Interface Sci.*, 2017, **495**, 1–8.

22 P. Karolia, D. Tiwari and R. Jain, Electrocatalytic sensing of omeprazole, *Ionics*, 2015, **21**(8), 2355–2362.

23 Z. Chomisteková, E. Culková, R. Bellová, D. Melicherčíková, J. Durdiak, J. Timko, M. Rievaj and P. Tomčík, Oxidation and reduction of omeprazole on boron-doped diamond electrode: Mechanistic, kinetic and sensing performance studies, *Sens. Actuators, B*, 2017, **241**, 1194–1202.

24 E. I. El-Kimary and A. A. Marwa Ragab, Recent Analytical Methodologies for the Determination of Omeprazole and/or Its Active Isomer Esomeprazole in Different Matrices: A Critical Review, *Crit. Rev. Anal. Chem.*, 2022, **52**(1), 106–130.

25 W. Jiang, L. Huang, D. Zhang, Y. Wang and G. Pan, Graphene-Based Composites for Electrochemical Sensor Fabrication and Their Application for Drug Detection, *Int. J. Electrochem. Sci.*, 2021, **16**, 21037.

26 A. Afkhami, A. Bahiraei and T. Madrakian, Gold nanoparticle/multi-walled carbon nanotube modified glassy carbon electrode as a sensitive voltammetric sensor for the determination of diclofenac sodium, *Mater. Sci. Eng. Carbon*, 2016, **59**, 168–176.

27 N. Baig, M. Sajid and T. A. Saleh, Recent trends in nanomaterial-modified electrodes for electroanalytical applications, *TrAC, Trends Anal. Chem.*, 2019, **111**, 47–61.

28 M. Ahmadi, A. Ghoorchian, K. Dashtian, M. Kamalabadi, T. Madrakian and A. Afkhami, Application of magnetic nanomaterials in electroanalytical methods: A review, *Talanta*, 2021, **225**, 121974.

29 J. M. Gonçalves, L. V. de Faria, A. B. Nascimento, R. L. Germscheidt, S. Patra, L. P. Hernández-Saravia, J. A. Bonacin, R. A. A. Munoz and L. Angnes, Sensing performances of spinel ferrites MFe_2O_4 (M = Mg, Ni, Co, Mn, Cu and Zn) based electrochemical sensors: A review, *Anal. Chim. Acta*, 2022, **1233**, 340362.

30 P. T. K. Thu, N. D. Trinh, N. T. V. Hoan, *et al.*, Synthesis of cobalt ferrite and simultaneous determination of ascorbic acid, acetaminophen and caffeine by voltammetric method using cobalt ferrite modified electrode, *J. Mater. Sci.: Mater. Electron.*, 2019, **30**, 17245–17261.

31 N. Q. Man, N. T. Thanh Tu, N. T. Vuong Hoan, H. X. Anh Vu, L. L. Son, N. D. Vu Quyen, D. N. Nhiem, N. H. Phong, V. T. Nguyen, T. N. Tuyen and D. Q. Khieu, Electrochemical determination of clenbuterol with nickel-ferrite/reduced-graphene-oxide-modified electrode, *J. Nanopart. Res.*, 2023, **25**, 31.

32 N. Tavakkoli, N. Soltani, F. Shahdost-fard, M. Ramezani, H. Salavati and M. R. Jalali, Simultaneous voltammetric sensing of acetaminophen, epinephrine and melatonin using a carbon paste electrode modified with zinc ferrite nanoparticles, *Microchim. Acta*, 2018, **185**, 479–499.

33 H. J. Kardile1, A. A. Pandit and K. M. Jadav, Hydrophilic nature of nickel ferrite thin film deposition by spray pyrolysis technique, *Int. J. Res. Biosci. Agric. Techn.*, 2021, **17**, 617–620.

34 A. Anosov, O. Koplak, E. Smirnova, E. Borisova, E. Korepanova and A. Derunets, Effect of Cobalt Ferrite Nanoparticles in a Hydrophilic Shell on the Conductance of Bilayer Lipid Membrane, *Membranes*, 2022, **12**, 1106.

35 A. Vedrtnam, K. Kalauni, S. Dubey and A. Kumar, A comprehensive study on structure, properties, synthesis and characterization of ferrites, *AIMS Mater. Sci.*, 2020, **7**, 800–835.

36 M. F. Huq, D. K. Saha, R. Ahmed and Z. H. Mahmood, Ni–Cu–Zn ferrite research: A brief review, *J. Sci. Res.*, 2013, **5**, 215–234.

37 M. Hashim, S. E. Shirsath, S. Kumar, R. Kumar, A. S. Roy, J. Shah and R. K. Kotnala, Preparation and characterization chemistry of nano-crystalline Ni–Cu–Zn ferrite, *J. Alloys Compd.*, 2013, **549**, 348–357.

38 A. D. Patil, R. A. Pawar, S. M. Patange, S. S. Jadhav, S. K. Gore, S. E. Shirsath and S. S. Meena, TiO_2-doped $Ni_{0.4}Cu_{0.3}Zn_{0.3}Fe_2O_4$ nanoparticles for enhanced structural and magnetic properties, *ACS Omega*, 2021, **6**(28), 17931–17940.

39 M. N. Akhtar, M. A. Khan, M. Raza, M. Ahmad, G. Murtaza, R. Raza, S. Shaukat, M. Asif, M. Saleem and M. Nazir, Structural, morphological, dielectric and magnetic characterizations of $Ni_{0.6}Cu_{0.2}Zn_{0.2}Fe_2O_4$ (NCZF/MWCNTs/PVDF) nanocomposites for multilayer chip inductor (MLCI) applications, *Ceram. Int.*, 2014, **40**(10), 15821–15829.

40 S. Zeki Bas, N. Yuncu, K. Atacan and M. Ozmen, A comparison study of MFe_2O_4 (M: Ni, Cu, Zn)-reduced graphene oxide nanocomposite for electrochemical detection of bisphenol A, *Electrochim. Acta*, 2021, **386**, 138519.

41 S. Sehrawat, M. Saini, A. Bhankhar and R. Shukla, A Comparative Analysis of Structural, Optical and Electrical Properties of Polyaniline/Ferrite (Co, Ni, Cu, Zn) Composites, *ECS J. Solid State Sci. Technol.*, 2022, **11**, 113005.

42 J. Han, L. Sun, E. Cao, W. Hao, Y. Zhang and L. Ju, Structural, magnetic, and dielectric properties of Ni–Zn ferrite and Bi_2O_3 nanocomposites prepared by the sol-gel method, *Chin. Phys. B*, 2021, **30**, 096102.

43 S. Tajik, Y. Orooji, Z. Ghazanfari, F. Karimi, H. Beitollahi, R. S. Varma, H. W. Jang and M. Shokouhimehr, Nanomaterials modified electrodes for electrochemical detection of Sudan I in food, *J. Food Meas. Charact.*, 2021, **15**(4), 3837–3852.

44 M. H. Omar, K. A. Razak, M. N. Ab Wahab and H. H. Hamzah, Recent progress of conductive 3D-printed electrodes based upon polymers/carbon nanomaterials using a fused deposition modelling (FDM) method as emerging electrochemical sensing devices, *RSC Adv.*, 2021, **11**(27), 16557–16571.

45 J. Li, S. Zhang, L. Zhang, Y. Zhang, H. Zhang, C. Zhang, X. Xuan, M. Wang, J. Zhang and Y. Yuan, A novel graphene-based nanomaterial modified electrochemical sensor for the detection of cardiac troponin I, *Front. Chem.*, 2021, **9**, 1–8.

46 S. Fu, Y. Zhu, Y. Zhang, M. Zhang, Y. Zhang, L. Qiao, N. Yin, K. Song, M. Liu and D. Wang, Recent advances in carbon nanomaterials-based electrochemical sensors for phenolic compounds detection, *Microchem. J.*, 2021, **171**, 106776.

47 M. Khan, M. N. Tahir, S. F. Adil, H. U. Khan, M. R. H. Siddiqui, A. A. Al-Warthan and W. Tremel, Graphene based metal and metal oxide nanocomposites: synthesis, properties and their applications, *J. Mater. Chem. A*, 2015, **3**, 18753–18808.

48 S. K. Kandasamy, Graphene oxide, in *Graphene, Nanotubes and Quantum Dots-Based Nanotechnology*, Woodhead Publishing, 2022, pp. 155–172.

49 H. Beitollahi, M. Safaei, M. R. Shishehbore and S. Tajik, Application of $Fe_3O_4@SiO_2/GO$ nanocomposite for sensitive and selective electrochemical sensing of tryptophan, *J. Electrochem. Sci. Eng.*, 2019, **9**(1), 45–53.

50 S. Amani, N. Sohrabi, R. Mohammadi and I. Ahadzadeh, Synthesis and investigation of $CoMnFeO_4$/reduced graphene oxide as ecofriendly electrode material for supercapacitor and its electrochemical performances, *J. Alloys Compd.*, 2023, **937**, 168020.

51 B. C. Behera, S. N. Sarangi, N. K. Sahoo, S. P. Dash and S. K. Tripathy, Magnetic Nanoparticles-Based Novel Sensors for Select Biomedical/Biological Science Applications, *Biomaterials-Based Sensors*, 2023, Vol. 1, pp. 325–348.

52 Y. Poo-arporn, S. Pakapongpan, N. Chanlek and R. P. Poo-arporn, The development of disposable electrochemical sensor based on Fe_3O_4-doped reduced graphene oxide modified magnetic screen-printed electrode for ractopamine determination in pork sample, *Sens. Actuators, B*, 2019, **284**, 164–171.

53 C. McKeever, S. Callan, S. Warren and E. Dempsey, Magnetic nanoparticle modified electrodes for voltammetric determination of propellant stabiliser diphenylamine, *Talanta*, 2022, **238**, 123039.

54 M. Vahidifar and Z. Es'haghi, Magnetic Nanoparticle-Reinforced Dual-Template Molecularly Imprinted Polymer for the Simultaneous Determination of Oxazepam and Diazepam Using an Electrochemical Approach, *J. Anal. Chem.*, 2022, **77**(5), 625–639.

55 M. Valian, A. Khoobi and M. Salavati-Niasari, Synthesis, characterization and electrochemical sensors application of $Tb_2Ti_2O_7$ nanoparticle modified carbon paste electrode for the sensing of mefenamic acid drug in biological samples and pharmaceutical industry wastewater, *Talanta*, 2022, 123593.

56 Y. Wang, H. Zhu, Y. Chen, X. Wu, W. Zhang, C. Luo and J. Li, Design of hollow $ZnFe_2O_4$ microspheres@graphene decorated with TiO_2 nanosheets as a high-performance low frequency absorber, *Mater. Chem. Phys.*, 2017, **202**, 184–189.

57 S. Kumar, R. Walia, A. Kumar and V. Verma, Hybrid structure of MWCNT/ferrite and GO incorporated composites for microwave shielding properties and their practical applications, *RSC Adv.*, 2021, **11**(17), 9775–9787.

58 Y. Li, D. Li, J. Yang, H. Luo, F. Chen, X. Wang and R. Gong, Enhanced microwave absorption and surface wave attenuation properties of $Co_{0.5}Ni_{0.5}Fe_2O_4$ fibers/reduced graphene oxide composites, *Materials*, 2018, **11**(4), 508–518.

59 Y. O. Al-Ghamdi, M. Jabli, M. H. Alhalafi, A. Khan and K. A. Alamry, Alamry Hybridized sulfated-carboxymethyl cellulose/MWNT nanocomposite as highly selective electrochemical probe for trace detection of arsenic in real environmental samples, *RSC Adv.*, 2023, **13**, 18382–18395.

60 S. Javanbakht, M. Pooresmaeil and H. Namazi, Green one-pot synthesis of carboxymethylcellulose/Zn-based metal-organic framework/graphene oxide bio-nanocomposite as a nanocarrier for drug delivery system, *Carbohydr. Polym.*, 2019, **208**, 294–301.

61 M. Pooresmaeil, H. Namazi and R. Salehi, Simple method for fabrication of metal-organic framework within a carboxymethylcellulose/graphene quantum dots matrix as a carrier for anticancer drug, *Int. J. Biol. Macromol.*, 2020, **164**, 2301–2311.

62 B. Borisova, A. Sánchez, S. Jiménez-Falcao, M. Martín, P. Salazar, C. Parrado, J. M. Pingarrón and R. Villalonga, Reduced graphene oxide-carboxymethylcellulose layered with platinum nanoparticles/PAMAM dendrimer/magnetic nanoparticles hybrids. Application to the preparation of enzyme electrochemical biosensors, *Sens. Actuators, B*, 2016, **232**, 84–90.

63 K. Juengchareonpoon, P. Wanichpongpan and V. Boonamnuayvitaya, Trimethoprim adsorption using graphene oxide-carboxymethylcellulose film coated on polyethylene terephthalate as a supporter, *Chem. Eng. Process.*, 2021, **169**, 108641.

64 C. Arenas, E. Sánchez-Tirado, I. Ojeda, C. Gómez-Suárez, A. González-Cortés, R. Villalonga, P. Yáñez-Sedeño and J. Pingarrón, An electrochemical immunosensor for adiponectin using reduced graphene oxide–carboxymethylcellulose hybrid as electrode scaffold, *Sens. Actuators, B*, 2016, **223**, 89–94.

65 A. Pendashteh, M. F. Mousavi and M. S. Rahmanifar, Fabrication of anchored copper oxide nanoparticles on graphene oxide nanosheets *via* an electrostatic coprecipitation and its application as supercapacitor, *Electrochim. Acta*, 2013, **88**, 347–357.

66 E. Sohouli, E. M. Khosrowshahi, P. Radi, E. Naghian, M. Rahimi-Nasrabadi and F. Ahmadi, Electrochemical sensor based on modified methylcellulose by graphene oxide and Fe_3O_4 nanoparticles: Application in the analysis of uric acid content in urine, *J. Electroanal. Chem.*, 2020, **877**, 114503–114513.

67 M. Yadav, K. Rhee, I. Jung and S. Park, Eco-friendly synthesis, characterization and properties of a sodium carboxymethyl cellulose/graphene oxide nanocomposite film, *Cellulose*, 2013, **20**(2), 687–698.

68 Y. Peng, C. Xia, M. Cui, Z. Yao and X. Yi, Effect of reaction condition on microstructure and properties of (NiCuZn) Fe_2O_4 nanoparticles synthesized *via* co-precipitation with ultrasonic irradiation, *Ultrason. Sonochem.*, 2021, **71**, 105369–105379.

69 H. Harzali, F. Saida, A. Marzouki, A. Megriche, F. Baillon, F. Espitalier and A. Mgaidi, Structural and magnetic properties of nano-sized NiCuZn ferrites synthesized by co-precipitation method with ultrasound irradiation, *J. Magn. Magn. Mater.*, 2016, **419**, 50–56.

70 F. Saida, H. Harzali, A. Marzouki, A. Mgaidi and A. Megriche, Effect of cobalt substitution on the structural and magnetic properties of nanopowders $Ni_{0.4}Cu_{0.2}Zn_{0.4}Fe_2O_4$ by hydrothermal method, *Chem. Afr.*, 2017, **19**, 26–33.

71 Y. He, C. Lei, Q. Lin, J. Dong, Y. Yu and L. Wang, Mössbauer and Structural Properties of La-Substituted $Ni_{0.4}Cu_{0.2}Zn_{0.4}Fe_2O_4$ Nanocrystalline Ferrite, *Sci. Adv. Mater.*, 2015, **7**, 1809–1815.

72 B. Liu, W. Wang, J. Wang, Y. Zhang, K. Xu and F. Zhao, Preparation and catalytic activities of $CuFe_2O_4$ nanoparticles assembled with graphene oxide for RDX thermal decomposition, *J. Nanopart. Res.*, 2019, **21**, 48.

73 A. Afkhami, H. Khoshsafar, H. Bagheri and T. Madrakian, Preparation of $NiFe_2O_4$/graphene nanocomposite and its application as a modifier for the fabrication of an electrochemical sensor for the simultaneous determination of tramadol and acetaminophen, *Anal. Chim. Acta*, 2014, **831**, 50–59.

74 B. Habibi, S. Pashazadeh, L. A. Saghatforoush and A. Pashazadeh, Direct electrochemical synthesis of the copper based metal-organic framework on/in the heteroatoms doped graphene/pencil graphite electrode: Highly sensitive and selective electrochemical sensor for

sertraline hydrochloride, *J. Electroanal. Chem.*, 2021, **888**, 115210–115222.

75 A. J. Bard and L. R. Faulkner, Fundamentals and applications: electrochemical methods, *Electrochem. Methods*, 2001, **2**(482), 580–632.

76 M. K. Bojdi, M. Behbahani, M. H. Mashhadizadeh, A. Bagheri, S. S. H. Davarani and A. Farahani, Mercapto-ordered carbohydrate-derived porous carbon electrode as a novel electrochemical sensor for simple and sensitive ultra-trace detection of omeprazole in biological samples, *Mater. Sci. Eng. Carbon*, 2015, **48**, 213–219.

77 C. Ferrag, M. Noroozifar and K. Kerman, Thiol functionalized carbon ceramic electrode modified with multi-walled carbon nanotubes and gold nanoparticles for simultaneous determination of purine derivatives, *Mater. Sci. Eng. Carbon*, 2020, **110**, 110568.

78 G. G. Mohamed, F. A. N. El-Dieny, S. M. Khalilz and A. S. El-Mohammad, Metal complexes of omeprazole. Preparation, spectroscopic and thermal characterization and biological activity, *J. Coord. Chem.*, 2009, **62**, 645–654.

79 C. Ferrag, M. Noroozifar and K. Kerman, Ultralight 3D Graphene Oxide Aerogel Decorated with Pd–Fe Nanoparticles for the Simultaneous Detection of Eight Biomolecules, *ACS Appl. Mater. Interfaces*, 2023, **15**, 27502–27514.

80 M. Nemakal, S. Aralekallu, I. Mohammed, M. Pari, K. V. Reddy and L. K. Sannegowda, Nanomolar detection of 4-aminophenol using amperometric sensor based on a novel phthalocyanine, *Electrochim. Acta*, 2019, **318**, 342–353.

81 S. Aralekallu, M. Palanna, S. Hadimani, K. P. CP, V. A. Sajjan, M. O. Thotiyl and L. K. Sannegowda, Biologically inspired catalyst for electrochemical reduction of hazardous hexavalent chromium, *Dalton Trans.*, 2020, **49**(42), 15061–15071.

82 H. M. Abumelha, A. Q. Alorabi, H. Alessa, N. A. Alamrani, A. Alharbi, A. A. Keshk and N. M. El-Metwaly, Novel Iron Oxide Nanoparticle-Fortified Carbon Paste Electrode for the Sensitive Voltammetric Determination of Atomoxetine, *ACS Omega*, 2023, **8**, 19006–19015.

83 S. Shahrokhian, M. Ghalkhani, M. Bayat and F. Ghorbani-Bidkorbeh, Voltammetric behavior and determination of trace amounts of omeprazole using an edge-plane pyrolytic graphite electrode, *Iran. J. Pharm. Res.*, 2015, **14**(2), 465–471.

84 V. Gallardo, M. López-Viota, J. Sierra and M. Ruiz, Spectrophotometric and chromatographic determination of omeprazole in pharmaceutical formulations, *Pharm. Dev. Technol.*, 2009, **14**(5), 516–523.

85 I. Al-Salloum and B. Al-Sabti, Stability study of esomeprazole in different packaging material using stability indicating validating HPLC method, *World J. Pharm. Pharm. Sci.*, 2019, **8**, 20–25.

86 P. Gupta and R. N. Goyal, A sensitive pyrolytic graphite sensor for determination of omeprazole in human blood plasma and pharmaceuticals, *J. Electrochem. Soc.*, 2014, **161**(4), H255–H259.

87 A. M. Qaisi, M. F. Tutunji and L. F. Tutunji, Acid decomposition of omeprazole in the absence of thiol:

88 a differential pulse polarographic study at the static mercury drop electrode (SMDE), *J. Pharm. Sci.*, 2006, **95**(2), 384–391.

89 A. Afkhami, S. Sayari, F. Soltani-Felehgari and T. Madrakian, $Ni_{0.5}Zn_{0.5}Fe_2O_4$ nanocomposite modified carbon paste electrode for highly sensitive and selective simultaneous electrochemical determination of trace amounts of mercury (II) and cadmium (II), *J. Iran. Chem. Soc.*, 2015, **12**(2), 257–265.

89 B. Habibi, S. Pashazadeh, L. A. Saghatforoush and A. Pashazadeh, A thioridazine hydrochloride electrochemical sensor based on zeolitic imidazolate framework-67-functionalized bio-mobile crystalline material-41 carbon quantum dots, *New J. Chem.*, 2021, **45**(32), 14739–14750.

90 M. Altuntaş, D. B. Altuntaş, S. Aslan, E. Yılmaz and E. Nalbant, Determination of Exogenous Adrenaline Levels in Patients Undergoing Cardiopulmonary Resuscitation, *ACS Omega*, 2023, **8**, 19425–19432.

91 H. F. Assaf, H. Salah, N. Hashem, M. Khodari and A. Toghan, Fabrication of an electrochemical sensor based on copper waste wire recycling and its application, *Sens. Actuators, A*, 2021, **331**, 112962.

92 N. El-Enany, F. Belal and M. Rizk, The alternating current polarographic behavior and determination of lansoprazole and omeprazole in dosage forms and biological fluids, *J. Biochem. Biophys. Methods*, 2008, **70**(6), 889–896.

93 A. Radi, Anodic voltammetric assay of lansoprazole and omeprazole on a carbon paste electrode, *J. Pharm. Biomed. Anal.*, 2003, **31**(5), 1007–1012.

94 J.-L. Yan, Electrochemical behavior and the determination of omeprazole using glassy carbon electrode, *J. Appl. Sci.*, 2006, **6**(7), 1625–1627.

95 K. Deng, X. Liu, C. Li, Z. Hou and H. Huang, An electrochemical omeprazole sensor based on shortened multi-walled carbon nanotubes-Fe_3O_4 nanoparticles and poly (2, 6-pyridinedicarboxylic acid), *Sens. Actuators, B*, 2017, **253**, 1–9.

96 A. Salimi, Z. Enferadi, A. Noorbakhash and K. Rashidi, Sensitive amperometric detection of omeprazole and pantoperazole at electrodeposited nickel oxide nanoparticles modified glassy carbon electrode, *J. Solid State Electrochem.*, 2012, **16**(4), 1369–1375.

97 K. R. Mahanthesha, B. E. K. Swamy and K. V. Pai, Poly (alizarin) Modified glassy carbon electrode for the electrochemical investigation of omeprazole: A voltammetric study, *Anal. Bioanal. Electrochem.*, 2014, **6**(2), 234–244.

98 S. McClean, E. O'kane, V. Ramachandran and W. Smyth, Differential pulse polarographic study of the degradation of H^+/K^+ ATPase inhibitors SK&F 95601 and omeprazole in acidic media and the subsequent reactions with thiols, *Anal. Chim. Acta*, 1994, **292**(1–2), 81–89.

99 K. Pandian, J. Kalayarasi and S. C. Gopinath, Metal-free Sulfur-doped graphitic carbon nitride-modified GCE-based electrocatalyst for the enhanced electrochemical determination of Omeprazole in Drug formulations and Biological Samples, *Biotechnol. Appl. Biochem.*, 2022, **69**(6), 2766–2779.